Quantitative evaluation of middle ear radiopacity in French bulldogs using X-ray imaging

Eisei Shimizu[1] ⓘ, Kazuya Kushida[2] ⓘ, Shunsuke Miyahara[3] ⓘ, Kodai Tashiro[1] ⓘ, Aritada Yoshimura[3] ⓘ, Shoma Sugi[1] ⓘ, Mizuki Tamazawa[1] ⓘ, Miu Matsumoto[1] ⓘ, Airi Kaneyama[1] ⓘ, Miki Shimizu[1] ⓘ, Ryuji Fukushima[2] ⓘ and Miori Kishimoto[1*] ⓘ

[1]*Cooperative Department of Veterinary Medicine, Tokyo University of Agriculture and Technology, Fuchu, Tokyo, Japan*
[2]*Koganei Animal Medical Emergency Center, Tokyo University of Agriculture and Technology, Koganei, Tokyo, Japan*
[3]*Animal Medical Center, Tokyo University of Agriculture and Technology, Fuchu, Tokyo, Japan*

Abstract

Background: Radiographic examination of the middle ear in French bulldogs can be challenging due to their small ear cavity and thick walls. Quantifying opacity on radiographic images is required to determine normal or abnormal results.

Aim: To quantify the radiographic opacity of the middle ear in French bulldogs and create a threshold for objective diagnosis.

Methods: A study was conducted on 32 French Bulldogs using radiographic images. Significant difference tests were performed on the ears of patients with unilateral and bilateral middle ear filling on computed tomography. A threshold was established for detecting left–right asymmetry in the same individuals. In addition, comparisons were made between the filling and nonfilling middle ear groups to establish a threshold of pixel values that could determine single middle ear filling and nonfilling for different patient images.

Results: Significant differences were observed in the left–right difference in max, left–right difference in max-ave, and left–right ratio of max-ave between unilateral and bilateral filling groups. The max-ave left–right ratio had the highest area under the curve value with a cutoff of 1.077% and 92.3% sensitivity. The item that showed a significant difference between middle ear groups with and without filling was corrected for nasopharyngeal pixel values with a cutoff of 1.028% and 85% sensitivity.

Conclusion: Pixel value ratios in the middle ear region can detect asymmetries in ear densities. The max value in the region compared to the same image's nasopharyngeal region can determine the filling. Combining individual ear evaluations and symmetry improves accuracy.

Keywords: French bulldog, Middle ear, Quantitative evaluation, X-ray imaging.

Introduction

Computed tomography (CT) and magnetic resonance imaging are the gold standard for diagnosing middle ear lesions in dogs (Garosi *et al*., 2003; Owen *et al*., 2004; Rohleder *et al*., 2006; Doust *et al*., 2007). However, radiography as a screening test for the middle ear is also an important imaging tool in primary care because tomographic studies may not be performed if no abnormalities are detected by radiography.

Radiographic examination of the middle ear mainly detects increased radiographic opacity and bone changes (e.g., bone destruction and hyperplasia) due to internal filling. However, radiographic opacity varies with the X-ray dose and amount of soft tissue in the head. The differences in anatomical structures among breeds further complicate the standardization of middle ear radiographic diagnosis.

The middle ear of French bulldogs is particularly difficult to read radiographically. This breed is a common cause of exudative otitis media (Milne *et al.* 2020; Töpfer *et al*., 2022). However, the small volume of the middle ear cavity and the thick walls of the middle ear in relation to the body size of French bulldogs (Mielke *et al*., 2017) make the objective assessment of radiographic opacity difficult. In such breeds, quantification of radiographic opacity is required to serve as an indicator of normal or abnormal radiographic opacity.

*Corresponding Author: Miori Kishimoto. Cooperative Department of Veterinary Medicine, Tokyo University of Agriculture and Technology, Fuchu, Tokyo, Japan. Email: *miori@cc.tuat.ac.jp*
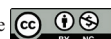
The present study aimed to quantify the radiographic opacity of the middle ear in French bulldogs and to create a threshold for objective diagnosis.

Materials and Methods

Sample images

We used the head X-ray and CT images of 32 French bulldogs. The collected subject data were as follows: age: 6 (0–13) years, weight: 10.9 (8.65–15.9) kg, 18 male and 14 female participants. CT examination showed middle ear disease in 30 of the 32 dogs. A rotating anode X-ray tube system (P13DK-85, Shimadzu, Kyoto, Japan) was used to produce the X-ray images, and an indirect conversion flat-panel detector (CALNEO Smart S77, Fujifilm Medical, Tokyo, Japan) and a digital imaging system (V station T, version 4.00, Fujifilm Medical) were used. The imaging conditions were as follows: tube voltage: 75–100 kV and tube current–exposure time product: 8 mAs. All CT images were acquired under general anesthesia. All imaging studies were performed on a 64-row detector CT system (Aquilion CXL, Canon Medical Systems, Tochigi, Japan). The imaging conditions were as follows: tube voltage: 120 kV, tube current: Auto exposure control (SD 10), imaging slice thickness: 0.5 mm, and rotation speed: 0.5 s/rotation.

Measurement of pixel values in the radiographic images

In digital X-ray systems, the X-ray dose detected by the flat-panel detector is recorded as a pixel value, which is a positive number that is zero or close to zero for pixels where no X-rays were detected, and is constant even if the window settings are changed on the DICOM viewer. The pixel values were measured using the histogram analysis function of the image processing workstation (Virtual Place Fujin, Canon Medical systems). The image processing application provided with the digital X-ray system and the image processing workstation used in this study can display the pixel values and the number of pixels in the selected region of interest (ROI) as a histogram. As no special operations are required, pixel values can be used easily in clinical practice.

A ROI was created by manually tracing the middle ear region on the dorsoventral image of the head among 32 patients (64 middle ears). The landmarks used for tracing were the tympanic opening of the auditory tube, the septum of the tympanic bullae, and the tympanic ring (Fig. 1). The maximum (max), average (ave), and minimum (min) pixel values were recorded from the histogram generated from the ROIs.

Study 1: Comparison of pixel values for the left and right middle ears in the same image

Given that X-ray images are transmissive and display multiple overlapping structures, the amount of change in pixel values in the middle ear region may not differ significantly between the normal and filled middle ears. Therefore, we first investigated whether the pixel values reflect unilateral or bilateral filling of the left and right middle ear on the images of the same individual. First, patients with filling in one side of the middle ear and on both sides on CT examination were categorized as the unilateral and bilateral filling groups, respectively.

Next, max-ave and ave-min were calculated from the max, ave, and min values of the left and right sides, respectively, obtained through a histogram analysis of the X-ray images. Finally, the left–right differences and ratios of max, ave, min, max-ave, and ave-min were calculated and tested for significant differences between the unilateral and bilateral filling groups. The threshold values were calculated using the receiver-operating characteristic (ROC) analysis for the items showing significant differences.

However, we excluded cases with an invaginated tympanic membrane (four patients) or ossification in the middle ear cavity (one patient) on CT images, which were difficult to distinguish from simple filling on the radiographic images. Two cases also had no filling in either the right or left middle ear, but these were also excluded because of the small sample size. As a result, 25 case images were assigned to the bilateral (12 cases) and unilateral (13 cases) filling groups.

Study 2: Individual assessment of the middle ear using pixel values

Next, we attempted to establish a pixel value threshold that could determine the filling and nonfilling of a single middle ear for different patient images, rather than for a left–right comparison of the same patient. However, the pixel values vary according to the X-ray dose detected with the flat-panel detector; it is impossible to simply create a threshold of the middle ear filling or nonfilling pixel values because they vary according to the dose and muscle mass of each individual patient. Therefore, it was necessary to divide the middle ear pixel value by the pixel value of another region in the image.

In the present study, circular ROIs were placed in the air (extracorporeal) or nasopharyngeal region (at the peripheral level of the sphenoid pterygoid process, Fig. 1) and the mean pixel values were measured and used as correction parameters. The values obtained by dividing the middle ear pixel values max, ave, and min by the air region were referred to as A-max, A-ave, and A-min, respectively, and the values obtained by dividing by the nasopharyngeal region were named N-max, N-ave, and N-min, respectively. The ears with middle ear filling on CT were assigned to the filling middle ear group, and those without middle ear filling were designated as the nonfilling middle ear group.

A-max, A-ave, A-min, N-max, N-ave, and N-min were calculated for each group, and significance difference tests were conducted between the two groups. Significant difference tests were also performed for uncorrected max, ave, min, max-ave, and ave-min. The threshold values were calculated through an ROC analysis for items showing significant differences.
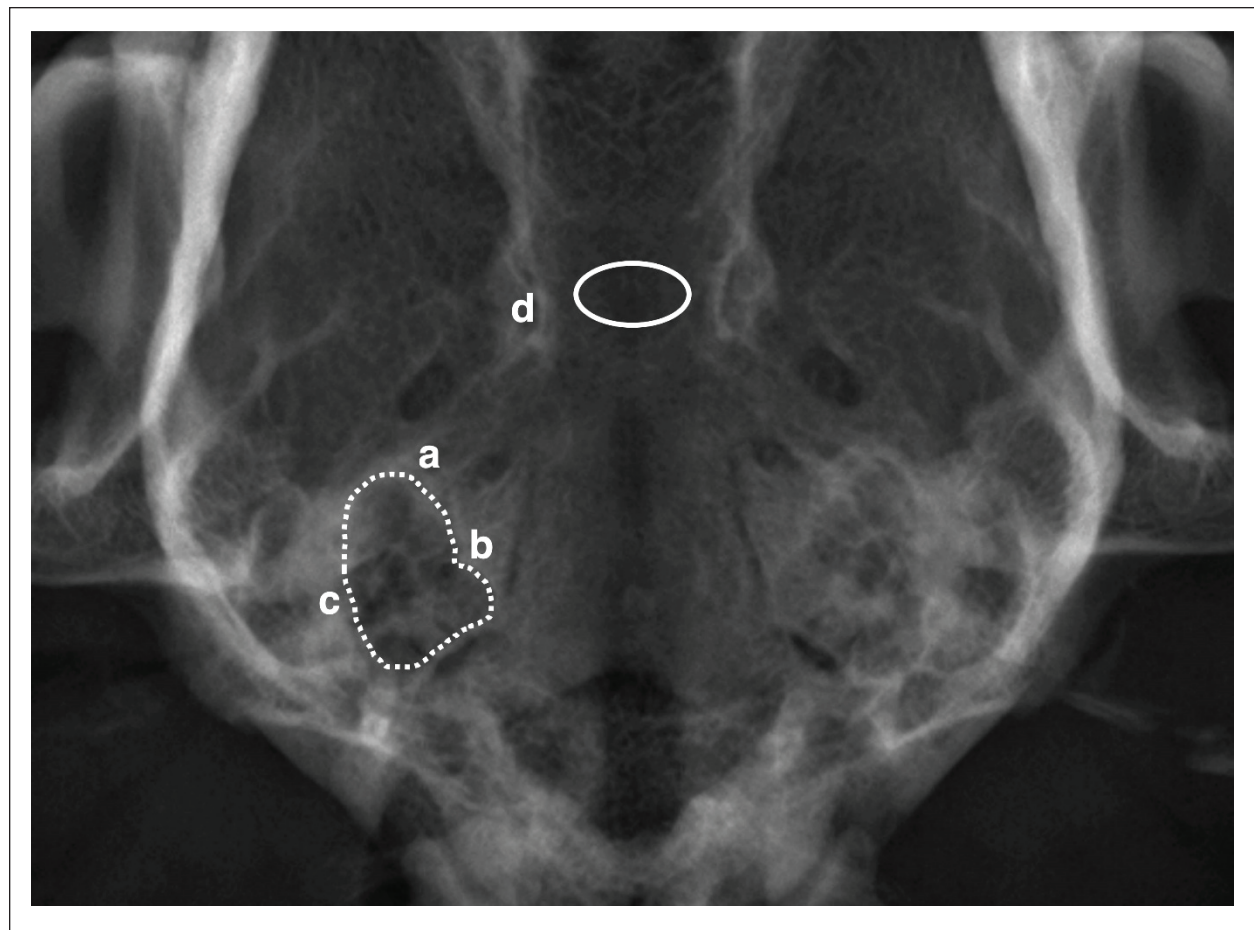
Fig. 1. The region of interest (ROI) was created by tracing the middle ear region of the head's dorsoventral image (broken circle). The landmarks used for tracing were the tympanic opening of the auditory tube (a), septum of tympanic bullae (b), and tympanic ring (c). The sphenoid process (d) was used as an anatomical landmark for ROI placement in the nasopharyngeal region. A circular ROI was placed at the peripheral level of the low X-ray absorption area sandwiched between the left and right sphenoid pterygoid processes (circle).

However, as in study 1, the middle ears that were difficult to distinguish from simple filling on radiographic images because of the presence of tympanic membrane invagination (four ears) or ossification in the middle ear cavity (one ear) on CT images were excluded. Air area correction was not considered for the four middle ears in the two cases with a small radiographic field and that did not contain sufficient air area. As a result, nasopharyngeal area correction was performed in the filled (40 ears) and unfilled (19 ears) middle ear groups. The air area correction was determined for the filling (37 ears) and nonfilling (18 ears) middle ear groups.

Statistical analysis

All statistical analyses were performed using statistical analysis software (SPSS, version 28.0, SPSS Inc, Chicago, IL). The Mann–Whitney U test was used to test for significant differences between the two groups, and the area under the curve (AUC) values were calculated for the ROC analysis. The AUC value in the ROC curve represents the model's accuracy, with values <0.70 indicating a fairly low accuracy, 0.70–0.90 indicating a somewhat useful accuracy, and 0.90–1.00 indicating an excellent accuracy (Swets, 1988). The Youden Index was used to calculate the cutoff values. The Overall Model Quality using SPSS was also recorded. The statistical significance level for all tests was set at <5%.

Ethical approval

Not needed for this study.

Results

Study 1: Comparison of pixel values for the left and right middle ears in the same image

The items that were significantly different between the unilateral and bilateral filling groups were the left–right difference in max, left–right difference in max-ave, and left–right ratio of max-ave (Table 1). The results of the ROC analysis for these three items are shown in

Table 2. The max-ave left–right ratio had the highest AUC value and overall model quality.

Study 2: Individual assessment of the middle ear using pixel values

There were no significant differences in the uncorrected max, ave, min, max-ave, and ave-min values between the filling and nonfilling middle ear groups. The results for the max, ave, and min corrected for air or nasopharyngeal area are shown in Table 3. The item showing a significant difference between the filling and nonfilling ear groups was N-max; the results of the ROC analysis of N-max are shown in Table 4. The cutoff values determined by the Youden Index were applied to 59 ears, excluding five ears with tympanic membrane entrapment or ossification in the middle ear cavity. As a result, six middle ears were judged to be false-positive (judged as filled when not filled) and five middle ears were false-negative (judged as unfilled when filled).

Discussion

French bulldogs have a thick middle ear wall (bone) and a narrow middle ear lumen, making the difference in opacity between normal and abnormal cases hard to see on radiographic images, even when the middle ear is full. However, the present study has shown that the pixel values reflect this minor change. The symmetry of the middle ear density in the same individual can be determined using the maximum pixel value in the middle ear region, max-ave difference between the left and right, or maximum ave ratio between the left and right. A threshold for assessing symmetry was also developed using ROC analysis. Considering the AUC value and sensitivity of the ROC analysis, the left–right ratio of max-ave may be the most accurate reflection of symmetry. Moreover, the absolute evaluation of individual middle ear concentrations was possible by dividing the max of the middle ear region by the pixel value of the nasopharyngeal region in the same image. In the present study, the max, ave, and min values of the ROI were selected as the measurement pixel values. As a result, the parameters using min (min and ave-min) did not show significant results in either the left–right evaluation or the individual evaluation. The highest absorbed dose (white on the image) in the ROI is defined as min. In other words, min varies even when the bone component is increasing because it reflects not only the filling but also the bone contrast. In some patients, the hyoid bone or the bony cerebellar tent may be strongly depicted in the middle ear region, and rolling during imaging may partially add to the craniocerebellar region's shadow. Contrarily, max reflects the air content. There is an artifact in which the absorbed dose is reduced by bone destruction in the

Table 1. Differences and ratios of the pixel values for both ears.

	Difference in pixel values between the middle ears[‡]				
	max–max	**ave–ave**	**min–min**	**(max-ave)–(max-ave)**	**(ave-min)–(ave-min)**
Bilateral filling ($n = 12$)	259 (0–727)	221 (6–982)	293 (25–494)	67.16 (6.333–699)	130.6 (8.333–1038)
Unilateral filling ($n = 13$)	619 (98–1279) *	174 (11–686)	219 (4–937)	293 (59–899) *	374 (22–1032)
	Ratio of pixel values for both middle ears [§]				
	max/max	**ave/ave**	**min/min**	**(max-ave)/(max-ave)**	**(ave-min)/(ave-min)**
Bilateral filling ($n = 12$)	1.052 (1.007–1.253)	1.029 (1.001–1.143)	1.056 (1.002–1.185)	1.052 (1.003–1.264)	1.081 (1.003–1.534)
Unilateral filling ($n = 13$)	1.028 (1000–1.084)	1.024 (1.000–1.144)	1.058 (1.000–1.269)	1.273 (1.043–1.524) †	1.242 (1.009–1.802)

Note: Max, ave, and min: maximum, average, and minimum pixel values of the region of interest, respectively. [‡]: difference between the larger and smaller values, [§]: ratio of the smaller value divided by the larger value. *:$p < 0.05$, †:$p < 0.01$.

Table 2. ROC analysis of the parameters with significant differences.

	Sensitivity (%)	Specificity (%)	Cutoff value	AUC	Overall model quality
max–max	46.2	100	747	0.782	0.6
max/max	61.5	83.3	257	0.782	0.6
(max-ave)/(max-ave)	92.3	66.7	1.077	0.853	0.71

Note: Max–max: difference in the maximum pixel values between both middle ears, max/max: ratio of maximum pixel values for both middle ears, (max-ave)/(max-ave): ratio of (maximum-average) pixel value for both middle ears, AUC: area under the curve.

Table 3. Parameters of the middle ears with and without filling.

	Without correction				
	max	**ave**	**min**	**max-ave**	**ave-min**
Nonfilling (*n* = 19)	12,360 (4,537–13,558)	10,821 (1,924–12,773)	8,386 (909–11,662)	1,467 (649–2,808)	2,317 (932–3,851)
Filling (*n* = 40)	10,861 (3,621–13,565)	9,513 (1,907–12,741)	6,840 (870–11,963)	1,660 (606–3,341)	2,073 (778–3,139)
	With air correction				
	A-max	**A-ave**	**A-min**		
Nonfilling (*n* = 18)	1.2849 (1.1863–1.6490)	1.4595 (1.2756–2.2727)	1.8787 (1.4533–4.3041)		
Filling (*n* = 37)	1.3456 (1.1955–1.7040)	1.5615 (1.2785–2.1941)	2.1535 (1.4197–3.2774)		
	With nasopharyngeal correction				
	N-max	**N-ave**	**N-min**		
Nonfilling (*n* = 19)	0.9645 (0.9448–0.9908)	1.0778 (1.0559–1.2718)	1.407 (1.2061–2.3959)		
Filling (*n* = 40)	1.0014 (0.9899–1.0416) *	1.2078 (1.0687–1.4399)	1.6368 (1.1927–2.1340)		

Note: Max, ave, and min: maximum, average, and minimum pixel values of the region of interest, respectively. $^*p < 0.01$.

Table 4. ROC analysis of the parameters with significant differences.

	Sensitivity (%)	**Specificity (%)**	**Cutoff value**	**AUC**	**Overall model quality**
N-max	85.0	63.2	1.028	0.745	0.61

Note: N-max: maximum pixel value of the middle ears corrected by the mean pixel value of the nasopharyngeal area. AUC: area under the curve.

middle ear. However, the significantly higher (black) pixel values in the ROI are likely to reflect the presence of air. As a result, the parameters using max (max and max-ave) are considered significant. In cases of middle ear disease, the significantly higher (black) pixel values are minute and cannot be detected visually. Therefore, measuring the pixel values is important.

The ave alone did not show significant results in either the left–right evaluation or the individual evaluation. The ave is the sum of each pixel value divided by the total number of pixels. When the histogram is leveled, the variation of pixel values is less pronounced in ave as compared with the variation of max values. Therefore, ave alone is considered to not reflect the changes in middle ear filling.

However, there are some limitations when using max-based indices. In the present study, max and max-ave were employed, and the left–right difference in max, left–right difference in max-ave, and left–right ratio in max-ave reflected the symmetry of the left and right middle ears. However, the left–right ratio of max was not significant. This may be due to the underestimation of the difference between the left and right pixel values due to high or low imaging doses. In the present study, the pixel values of the left and right middle ears were compared in the same image (study1), but the imaging

doses for each patient's image were not identical. The max value is higher for the images taken at higher doses. The higher the ratio of the values, the smaller the change rather than the difference, which makes it difficult to show the differences in the left and right pixel values (e.g., the lowest and highest max values for all middle ears used in this study were approximately 4,000 and 13,000, respectively). The left–right ratio is 0.89 when the left and right middle ear max values were 4,000 and 4,500, respectively. Contrarily, when the max values of the left and right middle ears were 13,000 and 13,500, respectively, the left–right ratio was 0.96. In both cases, the difference between the max values was 500, but the higher the dose, the closer the ratio approaches 1.0. Therefore, the left–right ratio of max should not be taken into account in the left–right comparisons.

Contrarily, the max-ave significantly reflected symmetry in both the left–right difference and left–right ratio. This may be due to the correction of numerical digits by dose in the process of subtracting the ave from the max. In this study, the sensitivity, AUC value, and overall model quality were the highest for the left–right ratio of max-ave. The cutoff values were also calculated. However, only two patients in this study had no filling in both middle ears on CT. This is due

to the small sample size and because French bulldogs are a predominant breed for developing otitis media. Therefore, the present study was unable to test the three groups with normal bilateral middle ears, one group with unilateral filling, and one group with bilateral filling. To obtain more accurate cutoff values, it is necessary to increase the sample size and include cases with bilateral normal middle ears in future studies.

In different patients, the pixel values obtained from each image cannot be compared among patients because of the differences in the imaging dose and body size. However, in the present study, the individual assessment of the middle ear was possible using cutoff values obtained using X-ray images of different patients by utilizing a correction value obtained by dividing the maximum value of the middle ear ROI by the average value of the nasopharyngeal ROI (study 2). The nasopharyngeal region is affected by the skull and soft tissues in the same way as the middle ear region; however, because it is a region separate from the middle ear, the histogram is allocated separately from the middle ear when creating the image. Therefore, the pixel values of the middle ear region may be corrected by the pixel values of the nasopharyngeal region to compensate for the differences in dose and soft tissue content. However, the correction in the air region did not produce significant results. This is thought to be because the histogram produced by direct X-rays that do not pass through the patient is separate from the main histogram produced by the patient's components and is therefore subject to automatic density correction when the digital image is produced.

In the present study, the nasopharyngeal region was used as the intrasubject area for correction, as the nasopharyngeal region is centrally located in the dorsoventral image of the head and is not excluded from the exposure field in any radiograph. Another reason is that the landmarks (at the level of the peripheral sphenoid pterygoid process) are clear and the measurements are highly reproducible. However, in the present study, no comparisons were made for other areas. Therefore, more areas may need to be studied to obtain more reliable corrected max values.

A sensitive cutoff value was obtained by using the max of the middle ear ROI corrected by the nasopharyngeal ROI. However, when 59 middle ears were classified as filled or unfilled using the cutoff value, 11 middle ears showed false positivity (six ears) or false negativity (five ears).

The causes of the false-positive results could not be determined. However, three reasons could be inferred. One is the shape of the middle ear. According to previous reports, French bulldogs' middle ears are more flat as compared to those of nonbrachycephalic breeds (Mielke *et al*., 2017). Therefore, individuals with more flattened ears have lesser air volume in the lumen, resulting in lesser transparency of the middle ear in the dorsoventral image of the head. In the present

study, four of the six false-positive middle ears were more severely flattened as compared to the others. The second factor is the thickness of the middle ear wall. A thick middle ear wall leads to narrowing of the lumen in addition to reduced transparency due to bone, leading to reduced transparency in the middle ear region on radiographic images. Particularly, French bulldogs have a thick middle ear wall, and the individual differences in the thickness of the wall require attention in radiological diagnosis. The thickness of the middle ear wall is also increased by bone augmentation induced by middle ear inflammation (Dickie *et al*., 2003; Gotthelf, 2004; Belmudes *et al*., 2018). False positives should be noted in patients with previous otitis media. The third type is bony malformations of the structures overlapping the middle ear region. In one case of false-positive middle ear, the parietal and occipital bone shadows overlapped with the middle ear shadows because of skull deformity, increasing the middle ear region's density. The presence or absence of anatomical features that deviate markedly from normal should be confirmed in the diagnosis.

The cause of the false-negative cases was considered to be reduced bone density in the middle ear region. The perforation of the middle ear walls or reduced bone density was observed in four of the five false-negative middle ears. Reduced bone density decreases the pixel value of the middle ear region. Therefore, false negativity should be noted in cases with middle ear wall destruction or bone thinning (Dickie *et al*., 2003; Foster *et al*., 2015; Belmudes *et al*., 2018; Krainer *et al*., 2021) due to chronic otitis media. Bone destruction of the tympanic opening of the auditory tube, septum of the tympanic bullae, and tympanic ring can be easily noted during tracing of the middle ear outline and may be useful in detecting false-negative cases due to the bone destruction in the middle ear.

Although the present study identified a cutoff value for the individual assessment of middle ear density using pixel values, the sensitivity was 85%, and false-positive and false-negative cases could not be excluded. This could be fatal, especially in cases of false-negative bilateral middle ears. To improve the diagnostic accuracy, one proposal has been made. After performing an individual assessment of the middle ear using N-max (pixel value of the middle ear ROI divided by the pixel value of the nasopharyngeal ROI), performing a left–right ratio of max-ave, which is used to compare the pixel values of the left and right middle ears, is recommended. The left–right ratio of max-ave had an AUC of 0.853 based on the ROC analysis and a sensitivity of 92.3% at a cutoff value of 1.077. Using this method, detecting at least one case of unilateral middle ear filling among the bilateral false-negative cases is considered possible.

The present study has limitations and measurement pitfalls. The first limitation is the small sample size. Although reliable ROC analysis results were obtained

for the comparison of the left and right middle ears and for individual assessments, the sensitivity and specificity were not 100%. Further studies are required to increase the number of cases and to include middle ears with various changes. The results of this study established a method for quantitatively determining the presence or absence of middle ear filling. However, it is not possible to determine whether the filling is a simple fluid effusion or a solid lesion such as a tumor. However, we believe that this method is useful as a basis for performing tomographic imaging that can determine these conditions. The measurement pitfall is the position at which the image used for the measurement was acquired. If the patient rolls, the image of the middle ear, which is the measurement object, changes. Rolling to the left or right, but especially forward and backward tilt, must be considered. If the patient's head is tilted backward or forward, the middle ear is enlarged and the shadow is extended in particular. The structures overlapping the middle ear also change. In the present study, a ventral–dorsal image of the head with the hard palate horizontal to the table was used; therefore, the images taken using the same technique should be used when using the cutoff values.

Conclusion

Pixel value ratios in the middle ear region can detect asymmetries in ear densities. The max value in the region compared to the same image's nasopharyngeal region can determine the filling. Combining individual ear evaluations and symmetry improves accuracy.

Conflict of interest

The authors declare that there are no conflicts of interest.

Author contributions

Shimizu (Eisei) and Kishimoto: conceptualization, methodology, validation, formal analysis, investigation, resources, data curation, writing—original draft, writing—review and editing, visualization. Kushida, Fukushima, Yoshimura, Sugi, Tamazawa, Tashiro, and Matsumoto: conceptualization, methodology, validation, investigation, resources, data curation, visualization. Miyahara, Kaneyama, and Shimizu (Miki): conceptualization, methodology, validation, formal analysis, investigation, resources, data curation, writing—review and editing, visualization, supervision, project administration.

Funding

Data availability

All data are available in the published manuscript.

References

Belmudes, A., Pressanti, C., Barthez, P.Y., Castilla-Castaño, E., Fabries, L. and Cadiergues, M.C. 2018. Computed tomographic findings in 205 dogs with clinical signs compatible with middle ear disease: a retrospective study. Vet. Dermatol. 29, 45-e20.

Dickie, A.M., Doust, R., Cromarty, L., Johnson, V.S., Sullivan, M. and Boyd, J.S. 2003. Comparison of ultrasonography, radiography and a single computed tomography slice for the identification of fluid within the canine tympanic bulla. Res. Vet. Sci. 75, 209–216.

Doust, R., King, A., Hammond, G., Cave, T., Weinrauch, S., Mellor, D. and Sullivan, M. 2007. Assessment of middle ear disease in the dog: a comparison of diagnostic imaging modalities. J. Small Anim. Pract. 48, 188–192.

Foster, A., Morandi, F. and May, E. 2015. Prevalence of ear disease in dogs undergoing multidetector thin-slice computed tomography of the head. Vet. Radiol. Ultrasound. 56, 18–24.

Garosi, L.S., Dennis, R. and Schwarz, T. 2003. Review of diagnostic imaging of ear diseases in the dog and cat. Vet. Radiol. Ultrasound. 44, 137–146.

Gotthelf, L.N. 2004. Diagnosis and treatment of otitis media in dogs and cats. Vet. Clin. North Am. Small Anim. Pract. 34, 469–487.

Krainer, D. and Dupré, G. 2021. Influence of computed tomographic dimensions of the nasopharynx on middle ear effusion and inflammation in pugs and French bulldogs with brachycephalic airway syndrome. Vet. Surg. 50, 517–526.

Mielke, B., Lam, R. and Ter Haar, G. 2017. Computed tomographic morphometry of tympanic bulla shape and position in brachycephalic and mesaticephalic dog breeds. Vet. Radiol. Ultrasound. 58, 552–558.

Milne, E., Nuttall, T., Marioni-Henry, K., Piccinelli, C., Schwarz, T., Azar, A., Harris, J., Duncan, J. and Cheeseman, M. 2020. Cytological and microbiological characteristics of middle ear effusions in brachycephalic dogs. J. Vet. Intern. Med. 34, 1454–1463.

Owen, M.C., Lamb, C.R., Lu, D. and Targett, M.P. 2004. Material in the middle ear of dogs having magnetic resonance imaging for investigation of neurologic signs. Vet. Radiol. Ultrasound. 45, 149–155.

Rohleder, J.J., Jones, J.C., Duncan, R.B., Larson, M.M., Waldron, D.L. and Tromblee, T. 2006. Comparative performance of radiography and computed tomography in the diagnosis of middle ear disease in 31 dogs. Vet. Radiol. Ultrasound. 47, 45–52.

Swets, J.A. 1988. Measuring the accuracy of diagnostic systems. Science 240, 1285–1293.

Töpfer, T., Köhler, C., Rösch, S. and Oechtering, G. 2022. Brachycephaly in French bulldogs and pugs is associated with narrow ear canals. Vet. Dermatol. 33, 214-e60.